ACS APPLIED MATERIALS & INTERFACES

Research Article

www.acsami.org

Meso-oblate Spheroids of Thermal-Stabile Linker-Free Aggregates with Size-Tunable Subunits for Reversible Lithium Storage

Da Deng*,† and Jim Yang Lee*,‡

†Department of Chemical Engineering & Materials Science, College of Engineering, Wayne State University, 5050 Anthony Wayne Drive, Detroit, Michigan 48202, United States

‡Department of Chemical & Biomolecular Engineering, Faculty of Engineering, National University of Singapore, 10 Kent Ridge Crescent, Singapore 119260

Supporting Information

ABSTRACT: The organization of nanoscale materials as building units into extended structures with specific geometry and functional properties is a challenging endeavor. Hereby, an environmentally benign, simple, and scalable method for preparation of stable, linker-free, self-supported, high-order 3D meso-oblate spheroids of CuO nanoparticle aggregates with size-tunable building nanounits for reversible lithium-ion storage is reported. In contrast to traditional spherical nanoparticle aggregation, a unique oblate spheroid morphology is achieved. The formation mechanism of the unusual oblate spheroid of aggregated nanoparticles is proposed. When tested for reversible lithium ion storage, the unique 3D meso-oblate spheroids of CuO nanoparticle aggregate demonstrated highly improved electrochemical performance (around ~600 mAh/g over 20 cycles), which could be ascribed to the nanoporous aggregated mesostructure with abundant crystalline imperfection. Furthermore, the size of building units can be controlled (12 and 21 nm were tested) to further improve their electrochemical performance.

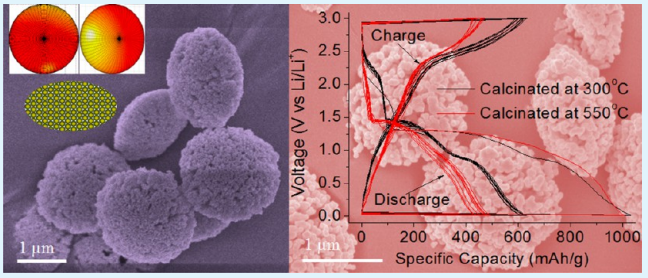

KEYWORDS: *CuO, aggregate, oblate-spheroid, linker-free, battery, anode*

1. INTRODUCTION

There is worldwide interest to improve performance of current lithium-ion batteries to satisfy the increasing demand for energy from mobile electronic devices, transportation section to large scale stationary energy storage. Recently, the interest has intensified after U.S. President Barack Obama's administration announced that the United States would be the first country to have one million electric vehicles on the road by 2015 (White House Press Release, January 26, 2010). After two decades of research, carbon as anode materials is approaching its theoretical capacity limit of 370 mAh/g and is still exclusively used currently. However, carbon-alternatives with higher capacity must be developed in order to further increase energy capacity. Pioneering study by Tarascon et.al. demonstrated that transition-metal oxides could be very promising substitutes for carbon in lithium ion batteries for high lithium storage capacity.[1] In particular, abundant and low-cost CuO with theoretical capacity of 674 mAh/g attract much attention, especially with the introduction of nanotechnology to improve cycling performance.[1−6]

Nanostructured CuO, in the form of nanoparticles, nanowires, and nanoplates has been demonstrated to show promising properties in reversible lithium ion storage.[1,3,7−9] The improved performance over bulk CuO could be attributed to shorter Li^+ diffusion path, good electrode−electrolyte contact, and improved strain tolerance.[10] However, nanoparticles with large surface area are difficult to package into a high-density bulk electrode.[10] Hence high-order three-dimensional (3D) structures of nanoscale building units (typically nanoparticles) may be used to deliver the advantages of nanoscale materials, meanwhile addressing the low bulk density and packaging issue.[10−14] However, the fabrication of organized high order 3D nanostructures with unique geometrical features and functional properties by simple methods is still a challenge. Most of the reported high-order assemblies depend on the use of linkers (e.g., surfactants, solvents, ligands, DNA, etc) to connect nanounits.[15−17] The lack of good thermal and mechanical stability limits their broader applications.[17−21] There have been a few reports on stable, linker-free, high-order nanostructures, but the morphology is normally limited to simple geometry.[11,22−24] The development of simple and scalable methodologies to fabricate linker-free, self-supporting stable 3D mesostructures in nonspherical geometries based on a high-order assembly of nanoscale building units remains a need and a challenge.

We report here an environmentally benign, simple, and scalable method for the preparation of 3D oblate spheroids constructed by CuO nanoparticles as building units. The

Received: October 31, 2013
Accepted: December 26, 2013
Published: December 26, 2013

preparation was based on the chemical transformation of a copper oxalate oblate spheroid precursor synthesized by a hydrothermal process. In contrast to conventional spherical nanoparticle aggregation, an unique oblate spheroid morphology was obtained here. The as-prepared oblate spheroids of CuO nanoparticle aggregate are highly stable and linker-free, and the building units of nanoparticles are size tunable. When preliminarily evaluated for reversible lithium ion storage, the oblate spheroids of CuO nanoparticle aggregate showed impressive capacity of 615 mAh/g with excellent cyclability.

2. EXPERIMENTAL SECTION

Materials Preparation. All chemicals were used as received. For a typical preparation, 30 mL of an aqueous solution of 0.2 M $H_2C_2O_4$ was added to 60 mL of a blue aqueous solution of 0.025 M $CuSO_4$ in a flask with stirring. The transparent blue mixture became turbid. The mixture was then transferred to a Teflon-lined autoclave reactor and kept in an electrical oven at 140−230 °C for 24 h before it was cooled down naturally. The blue sediment recovered was thoroughly washed with water and dried in a vacuum oven overnight. The blue powder was then calcined in air at 300 or 550 °C for 4 h to obtain a black powder and the color change also indicated the successful thermal conversion of copper oxalate to copper oxide.

Materials Characterization. All samples were characterized by field-emission scanning electron microscopy (FESEM) on a JEOL JSM-6700F operating at 5 kV, by transmission electron microscopy and selected area electron diffraction (TEM/SAED) on a JEOL JEM-2010F operating at 200 kV, by powder X-ray diffraction (XRD) on a Shimadu XRD-6000 using Cu K_α radiation, and by X-ray photoemission spectroscopy (XPS) on a KRATOS AXIS Hsi with Al K_α radiation.

Electrochemical Measurements. Eighty weight percent oblate spheroids of CuO nanoparticle aggregates was mixed with 10 wt % conductivity enhancer (Super-P carbon black, Timcal) and 10 wt % polyvinylidene fluoride (PVDF) binder in N-methylpyrrolidone (NMP) to a homogeneous slurry. The slurry was then applied to a copper disc current collector and dried in a vacuum oven at 120 °C. Electrochemical test cells were assembled in an argon-filled glovebox using the coated copper disc as the working electrode, lithium metal foil as the counter/reference electrode, and 1 M solution of $LiPF_6$ in a 50:50 w/w mixture of ethylene carbonate (EC) and diethyl carbonate (DEC) as the electrolyte. The cells were charged (lithiation) and discharged (delithiation) galvanostatically at room temperature in the 0.01−3 V voltage window on a battery tester.

2. RESULTS AND DISCUSSION

The overall morphology of the precursor of copper oxalate hydrate obtained from hydrothermal processing is clearly revealed by low magnification FESEM image shown a large number of mesoscale particles in Figure 1a. They are all in the shape of unique oblate spheroid tilted at certain degree against the SEM sample holder with the size about 1−3 μm. A high-magnification image (Figure 1b) of two representative mesoparticles in different orientations more clearly shows the oblate spheroid geometry. Close examination reveals the oblate spheroids have rough exterior "face" and irregular "edge". Here the terms "face" and "edge" are used in the sense defined and highlighted in Figure 1b. The image reveals that the "face" is formed by tips of nanorods and the "edge" is formed by sides of nanorods aggregated. Figure 1c shows another typical oblate spheroid standing perpendicularly on the sample holder, which more clearly reveals the "edge" formed by nanorods. The rough structures on the "face" and the rodlike structure at the "edge" indicate that the oblate spheroids are constructed from aggregated nanorods as units. The nanorod units are oriented perpendicular to "edge" as highlighted in Figure 1c. This

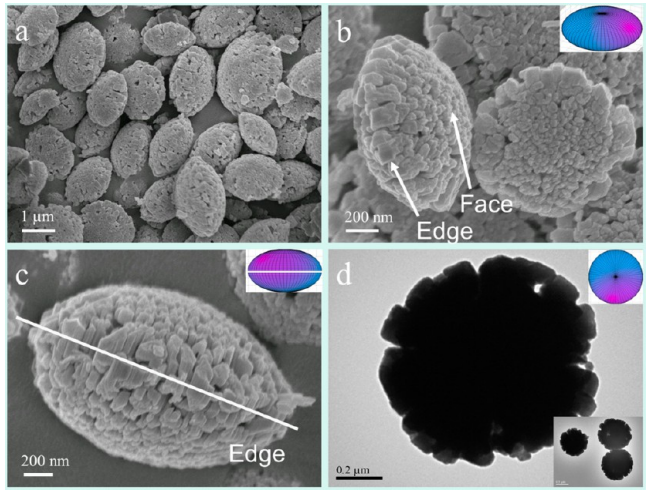

Figure 1. Electron microscope characterization of the meso-oblate spheroids of copper oxalate precursors prepared by hydrothermal method: (a) low-magnification FESEM image of overall morphology; (b) high-magnification image of two typical meso-oblate spheroids tilted at different degree, and the "face" and "edge" are defined as highlighted; inset shows an illustration of a tilted oblate spheroid; (c) side-view of a typical meso-oblate spheroid; inset shows the illustration of an oblate spheroid viewed from the edge; the "edge" is highlighted in white lines in the image and inset; (d) TEM image of a typical meso-oblate spheroid; lower inset shows three representative meso-oblate spheroids; upper inset shows an illustration of an oblate spheroid viewed from the face.

structure is further confirmed by TEM images. Figure 1d clearly outlines a typical oblate spheroid laying with "face" parallel to the sample holder, and the inset shows a few representative oblate spheroids. The edge of the oblate spheroid is not smooth due to that the nanorods are loosely packed around the edge. To more clearly show the geometry, drawings of oblate spheroids tilted at different degree obtained from Matlab are used to illustrate the morphology and orientation in the insets of Figure 1b−d (similar insets in Figures 4 and 5). An interesting phenomenon was observed in capturing the SAED pattern of the oblate spheroids. The diffraction spots disappeared quickly once the electron beam was focused onto the particles, suggesting the amorphization of the copper oxalate hydrate coordination compound under electron beam irradiation. This could be caused by dissociation of water molecules in the crystallites.

XRD analysis (Figure 2) revealed that the particles were phase-pure copper oxalate hydrates. All diffraction peaks could be indexed to $CuC_2O_4{\cdot}xH_2O$ according to JCPDS card No. 21−0297. The [110] diffraction peak is the strongest suggesting that the crystallites are stacked along the [110] and [1−10]

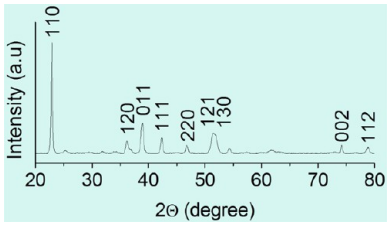

Figure 2. XRD pattern of meso-oblate spheroid precursor prepared by hydrothermal process.

dx.doi.org/10.1021/am404853n | ACS Appl. Mater. Interfaces 2014, 6, 1173−1179

directions. The preferential growth of grains of crystalline nanorod units may align in [001] axis direction given the linear one-dimensional sequence...$CuC_2O_4CuC_2O_4CuC_2O_4$....

Upon calcination in air at either 300 or 550 °C, the oblate spheroids of $CuC_2O_4.xH_2O$ could be successfully converted into CuO (by XRD analysis, Figure 3) maintaining the same

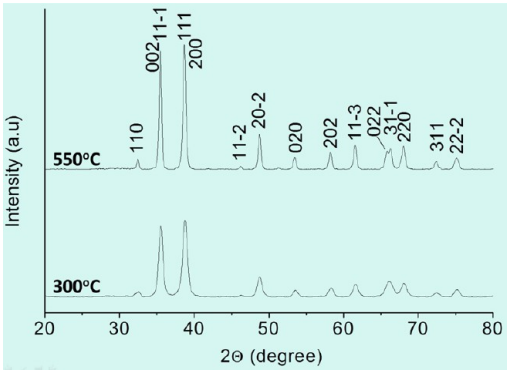

Figure 3. XRD patterns of the meos-oblate spheroids of CuO nanoparticle aggregates obtained by calcination at 300 °C (lower pattern) and 550 °C (upper pattern) in air of the precursor.

overall morphology with no significant change in mesoscale size of aggregates. The basic building nanounits are nanoparticles (by electron microscope, Figures 4 and 5). XRD analysis provided the evidence for the successful transformation into CuO (Figure 3). All XRD peaks of the calcined products could be indexed to CuO according to standard JCPDS card No 48−1548, indicating high phase purity and complete decomposition of $CuC_2O_4{\cdot}xH_2O$ into CuO under the experimental conditions. The size of CuO nanocrystallite calculated based on the Scherrer equation using (111) diffraction was about 12 and 21 nm for oblate spheroids obtained by calcination at 300 and 550 °C, respectively. The fact that oblate spheroids of CuO nanoparticle aggregate were obtained by calcination and there were no change in meso-structures suggests it is thermally stable. It was also mechanically robust against intense ultrasonication, which was used during the sample preparation for electron microscopy.

The low-magnification FESEM images at different magnification (Figure 4a and the inset) of CuO nanoparticle aggregates obtained by calcination in air at 300 °C clearly reveal that the heat treatment did not alter the overall morphology of oblate spheroids succeeded from its precursors. In another word the calcination product basically inherited the morphology of its mesoscale precursor shown in Figure1 and the precursor functioned as templates. High magnification FESEM image (Figure 4b) of a typical CuO mesoparticle tilted against the sample holder more clearly shows the preservation of the precursor morphology with both "edge" and "face" observed as its precursor. At the same time, the enlarged image also clearly reveals tiny CuO nanoparticles as the building nanounits that aggregated and distributed through the oblate spheroids. The morphology and presence of CuO nanoparticles in the oblate spheroids was also evidenced by low magnification TEM (Figure 4c). The clear oblate spheroid parentage indicates that the precursor could self-template the aggregation of CuO nanoparticles. The nonuniform distribution of the CuO nanounits around the "edge" in the oblate spheroids gave rise to nonuniform contrast in the TEM image, which agreed with that observed from precursor in Figure 1d. The building units

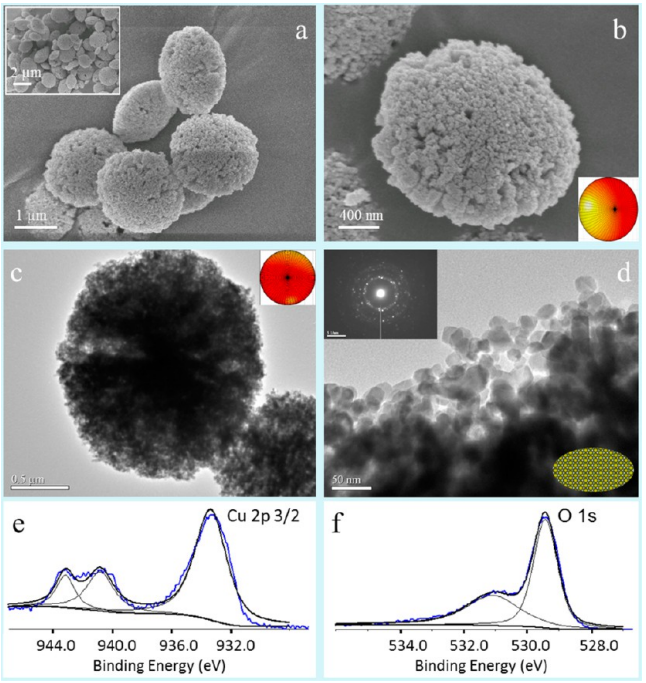

Figure 4. Calcination condition: 300 °C in air. FESEM images of the meso-oblate spheroids of CuO nanoparticle (~12 nm) aggregates: (a) a few typical meso-oblate spheroids tilted at different degree; inset shows low-magnification overall view; (b) high-magnification view of a representative meos-oblate spheroid; inset shows an illustration of a tilted oblate spheroid. TEM images of (c) a typical meso-oblate spheroid of CuO nanopartical aggregate; inset shows the illustration of an oblate spheroid view from the face; (d) high-magnification view more clearly shows the building units of CuO nanoparticles; upper and lower inset of d show the SAED pattern and illustration of aggregate viewed from edge respectively. XPS analysis results of (e) Cu 2p and (f) O 1s spectra of the meso-oblate spheroids of CuO nanoparticle aggregate.

of CuO nanoparticles are more clearly showed by high magnification TEM image (Figure 4d) of the edge of the oblate spheroids and they are about 12 nm in size, in good agreement with the XRD determination. The inset shows SAED pattern, with a hybrid of discrete diffraction spots and continuous rings which all could be assigned to crystalline CuO, indicating that the nanoparticles were crystalline and were aggregated disorderly in the meso-oblate spheroids. The completeness of the conversion reaction and phase purity of the CuO product were further demonstrated by XPS analysis. Figure 4e shows the high-resolution Cu $2p_{3/2}$ XPS spectrum where the main peak at 933.4 eV and the two satellite peaks 7.4 and 9.7 eV above due to multiplet splitting are typical Cu^{2+}.[4] Figure 4f shows the O 1s XPS spectrum that could be resolved into two component peaks at 529.4 and 531 eV. The dominant lower energy peak at 529.4 eV could be assigned to O^{2-} in CuO and the higher energy peak to adsorbed O on CuO nanoparticle aggregates.[4]

Furthermore, it was found that the size of the CuO nanoparticle building units could be easily tuned while keeping the unique mesoscale morphology of oblate spheroids by adjusting calcination temperature. This could be a convenient mean to vary the size-dependent properties of the nanostructured material. The products obtained from precursors calcined at 550 °C in air are shown in Figure 5. The low-magnification FESEM images (Figure 5a and the inset) show

dx.doi.org/10.1021/am404853n | ACS Appl. Mater. Interfaces 2014, 6, 1173−1179

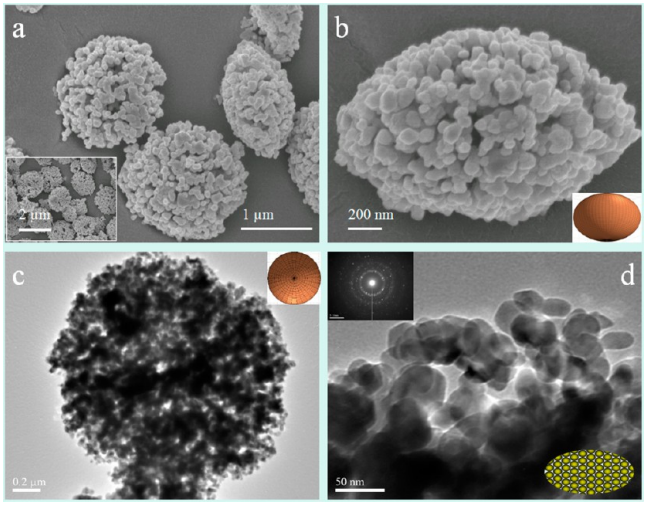

Figure 5. Calcination conditions: 550 °C in air. FESEM images of the meso-oblate spheroids of CuO nanoparticle (~21 nm) aggregates: (a) a few typical meso-oblate spheroids tilted at different degree; inset shows low-magnification overall view; (b) high-magnification view of a representative meos-oblate spheroid; inset shows an illustration of a tilted oblate spheroid. TEM images of (c) a typical meso-oblate spheroid of CuO nanopartical aggregate, inset shows the illustration of an oblate spheroid view from the face; (d) high-magnification view clearly shows the building units of CuO nanoparticles; upper and lower inset of (d) show the SAED pattern and illustration of aggregate viewed from edge.

the preservation of overall morphology of oblate spheroids at mesoscale, similar to those obtained at 300 °C calcination, but with bigger nanounits. The much rougher "face" and "edge" of the oblate spheroids revealed that the CuO nanoparticle building units were significantly larger than those formed by calcination in air at 300 °C (Figure 4). High-magnification FESEM image (Figure 5b) of a typical standing oblate spheroid viewed from the "edge" and the TEM image (Figure5c) viewed from the "face" both clearly show the packaging of the CuO nanoparticles in the aggregate. The building units of CuO nanoparticles and their aggregation in the oblate spheroid are more clearly observed by high magnification TEM image (Figure 5d). The CuO nanounits have size about 21 nm, which again is in good agreement with XRD determination. It is interesting to note that CuO nanoparticles in both cases as revealed by high-magnification TEM are not perfect spheres, which could contribute to stable nanoparticle aggregation. Nonspherical contact between the nanoparticles allows more contact points and hence stronger interparticle interaction. The inset of Figure 5d shows the SAED pattern which is almost the same as that obtained from calcination at 300 °C, indicating disorderly assembly of crystalline CuO nanounits. The phenomenon of that an increase in calcination temperature promoting the increase in size of nanoparticle units could be understood in terms of the Schott equation ($D = A\exp(-E/RT)$, where D is the particle size, E is the activation energy for crystal growth, A is a constant, and R is the ideal gas constant). It was estimated from Schott equation that the activation energy E for CuO nanounits is about 8.8 kJ/mol. Although only two temperature levels were used in the experiments, it is expected that the size of the CuO basic units could be easily varied by different temperatures without changes in the overall morphology.

Aside from the calcination temperature, other experimental variables such as concentration of reactants and reaction temperature and time in the hydrothermal synthesis were investigated as listed in Table S1 in the Supporting Information. The structure of products formed under different hydrothermal conditions and their corresponding products of calcination at 300 °C are shown in Figure S1 in the Supporting Information. In general, the interesting mesoscale oblate spheroid morphology prevailed under all combinations of the experimental variables within the specified ranges. There were, however, some differences between the products upon closer examination. An increase in the concentration of $CuSO_4$ or $H_2C_2O_4$ while keeping other variables fixed made the oblate spheroids "smoother" at the "edge" (Figure S1a, c in the Supporting Information). This could be due to the faster nucleation and formation of shorter or smaller nanorod units, which allow for more compact aggregation. On the other hand, increase in the hydrothermal temperature alone could flatten the "face" of oblate spheroids (see Figure S1e in the Supporting Information). This could be due to the packing of longer nanorod units from faster nanorod growth. The corresponding calcination product (see Figure S1f in the Supporting Information) showed many defects in the oblate spheroids, which more clearly revealed the internal structure. There was little morphology change when the hydrothermal processing time was doubled to 48h (Figure S1g in the Supporting Information), indicating that the oblate spheroids, once formed, were stable without further growth over time although the crystallinity may be improved. The XRD analysis (see Figure S2 in the Supporting Information) of the corresponding products after calcination in air at 300 °C indicated that all were phase-pure CuO. From the variations in peak intensities and peak width, it could be concluded that the crystallinity of the CuO building nanounits was improved with an increase in hydrothermal temperature or reaction time.

On the basis of the above experimental observations, a plausible mechanism for formation of oblate spheroids of CuO nanoparticle aggregate is provided as Scheme 1. When oxalate

Scheme 1. Proposed Formation Mechanism and Stage of Growth

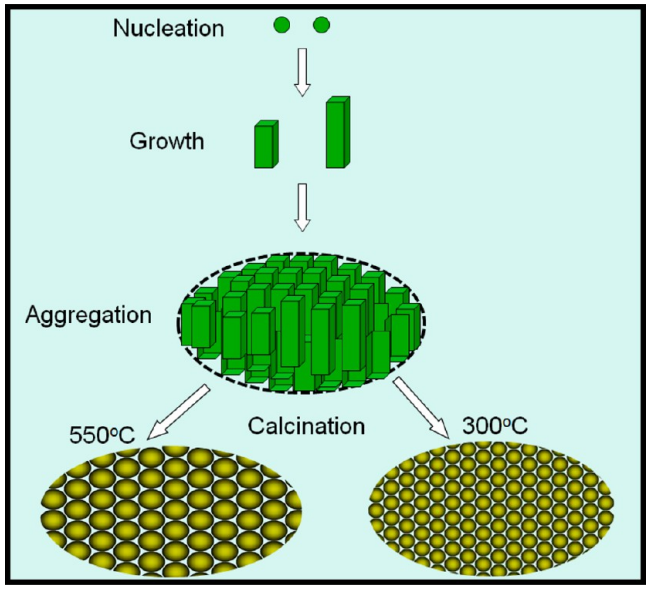

dx.doi.org/10.1021/am404853n | ACS Appl. Mater. Interfaces 2014, 6, 1173−1179

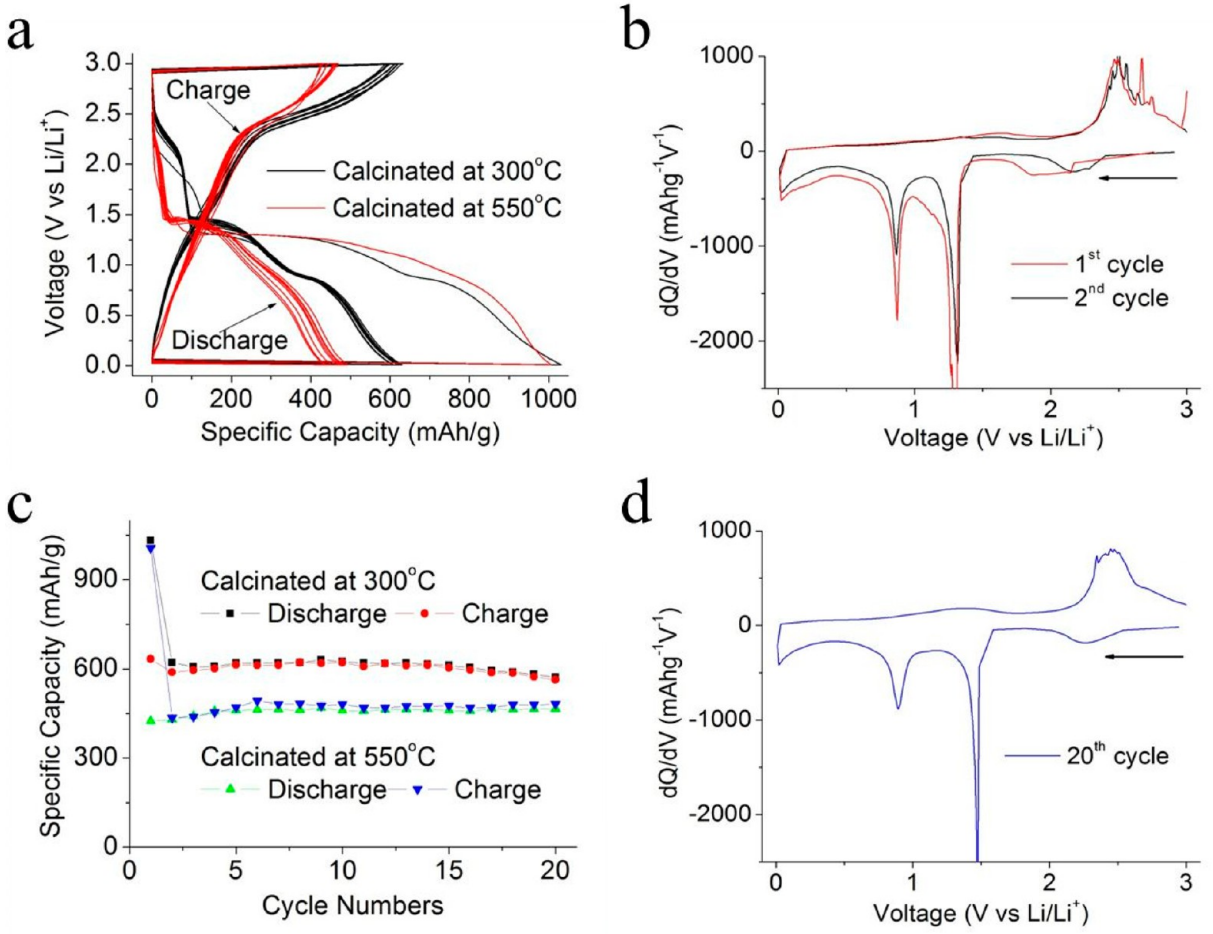

Figure 6. Electrochemical performance of the meso-oblate spheroids of CuO nanoparticle aggregate in reversible lithium ion storage: (a) First ten cycles of charge−discharge profiles of the CuO samples obtained by calcination at 300 (nanounit size, 12 nm; black) and 550 °C (21 nm red). (b) Differential charge−discharge capacity vs voltage plots for the first two cycles. (c) Specific capacity vs cycle number plots of the CuO samples obtained at 300 and 550 °C of calcination. (d) Differential charge−discharge capacity plot for the 20th cycle. Test conditions: current rate 100 mA/g, voltage window 0.01−3 V..

ions were mixed with copper ions, the precipitation of low solubility copper oxalate occurred in the aqueous solution according to the classical nucleation theory. It should be noted that oxalate ions have a planar structure; the presence of copper ions between adjacent oxalate ions could align the latter into a one-dimensional structure with the sequence ...Cu-C_2O_4CuC_2O_4CuC_2O_4... Because of to the different surface free energy of the different faces of the 1D structure, the surfaces interacted specifically to reduce the system free energy. Experimental observation of that the nanorod units were aligned in the direction of the short axis of oblate spheroids suggests that the side faces of nanorods were higher in surface energy and sideway aggregation was used to reduce the total free energy. However, the exact mechanism still requires further investigation.

During the subsequent calcination in air, the copper oxalate precursor decomposed into oblate spheroids of CuO according to the following reaction

$$CuC_2O_4 \cdot xH_2O \rightarrow CuO + CO + CO_2 + xH_2O$$

The release of gases during the decomposition reaction led to greater porosity in the aggregate, and the nanoparticles formed stayed as aggregate. The meso-oblate spheroid copper oxalate precursor also templated the aggregation of the nanoparticles to follow the morphology of the precursor. It should be noted that the number density of Cu atoms in $CuC_2O_4.xH_2O$ crystal structure is much lower than that in CuO. Hence the CuO phase obtained from the topotacitic transformation within the same mesoscale size range should contain more interior void than its precursor, just as experimentally observed. With different calcination temperature, the size of CuO nanounits could be controlled by temperature of calcination. In principle, this method of preparation leading to formation of mesoscale oblate spheroids of nanoparticle aggregation may be generic and could be applicable to other metal oxides.

The potential application of those mesoscale oblate spheroids of CuO nanoparticle aggregate as anode materials for lithium ion batteries was evaluated. Figure 6a shows the first 10 cycles of charge−discharge profiles of the two CuO samples calcined at 300 (black line) and 550 °C (red line). The first cycle discharge and charge capacities of the CuO oblate spheroids calcined at 300 °C were at 1031 and 634 mAh/g, respectively, whereas the corresponding values for the 550 °C calcined sample were 1006 and 425 mAh/g. The first cycle irreversible capacity loss could be generally attributed to solid-electrolyte interphase (SEI) formation from degradation of electrolyte and the irreversible trapping of Li^+ ions in those nanopores by possible interfacial lithium storage, which is hard

dx.doi.org/10.1021/am404853n | ACS Appl. Mater. Interfaces 2014, 6, 1173−1179

to extract.[2,3,8,9,13,25−28] The second to tenth cyclea of charge−discharge curves are nearly superimposable, indicating highly reversible lithium-ion storage properties. The two samples demonstrated almost the same charge−discharge profiles, indicating the same electrochemical reactions involved as expected. However, the sample with smaller size nanounits (12 nm) obtained by calcination at 300 °C has higher capacity than that with large nanounits (21 nm) calcined at 550 °C. This could be ascribed to that the former with smaller nanounits calcined at lower temperature possess abundant crystalline imperfection, grain boundary, and oxygen vacancies, which provides more additional Li intercalation positions.[29,30]

To better understand the electrochemical reactions involved, we plotted differential capacity vs voltage profiles of the first two charge−discharge cycles (Figure 6b). There are two distinctive reduction peaks at 0.9, and 1.3 V and broad peaks around 2.2−1.8 V in the first discharge cycle. The first cycle reduction peak around 2.1 V could be assigned to the complex reaction of partial reduction of CuO to $[Cu^{II}_{1-x}Cu^{I}_{x}]O_{1-x/2}$, whereas the voltages plateaus around 1.3 and 0.9 V could be assigned to multistep electrochemical reactions for insertion of Li into the CuO crystal lattice.[4,7,27] Those reduction peaks were observed again in the second cycle as expected, indicating reversible reactions. The first cycle reduction peak around 1.8 V could be assigned to the formation SEI arising from degradation of electrolyte,[26,27] and reduction of a trace adsorbed O_2/H_2O on CuO surface.[30] This peak disappeared in the second cycle onward and contributed to the first cycle irreversible capacity loss. For the oxidization process, there is a main peak around 2.5 V with small satellite peaks, which could be assigned to the Li^+ extraction from the crystal lattice of CuO.[3,29,30] The overall electrochemical reaction could be $CuO + 2Li^+ + 2e^- \leftrightharpoons Cu + Li_2O$.

Figure 6c shows the cycling performance of two CuO meso-oblate spheroid samples with building nanounits at different size obtained at different temperature. Both samples demonstrate higher specific capacity than carbon anode with practical capacity of 350 mAh/g. The preliminary cycling performance is improved with minimum capacity fading as compared to disordered CuO nanoparticles reported in literature.[2,4,31−33] The CuO oblate spheroids with building nanounits at size of 12 nm demonstrated higher capacity, while the other sample with building nanounits at size of 21 nm demonstrated better capacity retention. This observation suggests that there may be an optimum size to achieve the best balance between capacity and cyclability. After 20 cycles, capacity of 571 mAh/g still can be maintained, or only 7% fading as compared to initial cycle. The excellent capacity retention is further evidenced by differential charge−discharge capacity vs voltage plot for the 20th cycle (Figure 6d). The reduction and oxidization peaks corresponding to insertion and extraction of Li in and out of CuO anode are similar as those discussed above, and there is no significant drop of intensity in those redox peaks as compared to second cycle (Figure 6b). This also indirectly suggested that the mesostructure is stable and all the CuO building nanounits are still actively involved in reversible lithium ion storage.

3. CONCLUSION

In summary, stable, linker-free, high-order 3D meso-oblate spheroids of CuO nanoparticle aggregate with size-tunable building nanounits were successfully prepared by an environmentally benign, simple, and scalable method and fully characterized. In contrast to traditional spherical aggregation of nanoparticles, unique morphology of oblate spheroid was achieved here, and the size of basic building nanounits can be controlled by temperature. Various experimental conditions were carried out and the formation mechanism was proposed. When tested for reversible lithium-ion storage, the unique high-order 3D meso-oblate spheroids demonstrated highly improved electrochemical performance in terms of capacity and cyclability. Electrochemical analysis revealed that meso-oblate spheroids with smaller units of CuO nanoparticles obtained at lower temperature had better performance because of their abundant crystalline imperfection and grain boundary. However, more work is still needed.

■ ASSOCIATED CONTENT

Ⓢ Supporting Information

Experimental results obtained under other conditions and their corresponding FESE and XRD characterization; Matlab code for illustration. This material is available free of charge via the Internet at http://pubs.acs.org.

■ AUTHOR INFORMATION

Corresponding Authors

*E-mail: da.deng@wayne.edu.
*E-mail: cheleejy@nus.edu.sg.

Notes

The authors declare no competing financial interest.

■ REFERENCES

(1) Poizot, P.; Laruelle, S.; Grugeon, S.; Dupont, L.; Tarascon, J. M. *Nature* **2000**, *407*, 496.
(2) Zhang, X. J.; Zhang, D. G.; Ni, X. M.; Zheng, H. G. *Solid-State Electron.* **2008**, *52*, 245.
(3) Wang, H. B.; Pan, Q. M.; Zhao, H. W.; Yin, G. P.; Zuo, P. J. *J. Power Sources* **2007**, *167*, 206.
(4) Morales, J.; Sanchez, L.; Martin, F.; Ramos-Barrado, J. R.; Sanchez, M. *Electrochim. Acta* **2004**, *49*, 4589.
(5) Wang, X.; Tang, D.-M.; Li, H.; Yi, W.; Zhai, T.; Bando, Y.; Golberg, D. *Chem. Commun.* **2012**, *48*, 4812.
(6) Zhang, W.; Li, M.; Wang, Q.; Chen, G.; Kong, M.; Yang, Z.; Mann, S. *Adv. Funct. Mater.* **2011**, *21*, 3516.
(7) Zheng, S. F.; Hu, J. S.; Zhong, L. S.; Song, W. G.; Wan, L. J.; Guo, Y. G. *Chem. Mater.* **2008**, *20*, 3617.
(8) Zhang, X. J.; Zhang, D. G.; Ni, X. M.; Song, J. M.; Zheng, H. G. *J. Nanopart. Res.* **2008**, *10*, 839.
(9) Pan, Q.; Jin, H.; Wang, H.; Yin, G. *Electrochim. Acta* **2007**, *53*, 951.
(10) Bruce, P. G.; Scrosati, B.; Tarascon, J. M. *Angew. Chem., Int. Ed.* **2008**, *47*, 2930.
(11) Deng, D.; Lee, J. Y. *Chem. Mater.* **2008**, *20*, 1841.
(12) Lou, X. W.; Deng, D.; Lee, J. Y.; Feng, J.; Archer, L. A. *Adv. Mater.* **2008**, *20*, 258.
(13) Nam, K. T.; Kim, D. W.; Yoo, P. J.; Chiang, C. Y.; Meethong, N.; Hammond, P. T.; Chiang, Y. M.; Belcher, A. M. *Science* **2006**, *312*, 885.
(14) Arico, A. S.; Bruce, P.; Scrosati, B.; Tarascon, J. M.; Van Schalkwijk, W. *Nat. Mater.* **2005**, *4*, 366.
(15) Nykypanchuk, D.; Maye, M. M.; van der Lelie, D.; Gang, O. *Nature* **2008**, *451*, 549.
(16) Wang, X.; Zhuang, J.; Peng, Q.; Li, Y. D. *Nature* **2005**, *437*, 121.
(17) Lopes, W. A.; Jaeger, H. M. *Nature* **2001**, *414*, 735.
(18) Warren, S. C.; Messina, L. C.; Slaughter, L. S.; Kamperman, M.; Zhou, Q.; Gruner, S. M.; DiSalvo, F. J.; Wiesner, U. *Science* **2008**, *320*, 1748.
(19) Klajn, R.; Bishop, K. J. M.; Fialkowski, M.; Paszewski, M.; Campbell, C. J.; Gray, T. P.; Grzybowski, B. A. *Science* **2007**, *316*, 261.

(20) Boal, A. K.; Ilhan, F.; DeRouchey, J. E.; Thurn-Albrecht, T.; Russell, T. P.; Rotello, V. M. *Nature* **2000**, *404*, 746.
(21) Li, M.; Schnablegger, H.; Mann, S. *Nature* **1999**, *402*, 393.
(22) Liu, B.; Zeng, H. C. *J. Am. Chem. Soc.* **2004**, *126*, 16744.
(23) Jia, Z.; Yue, L.; Zheng, Y.; Xu, Z. *Mater. Res. Bull.* **2008**, *43*, 2434.
(24) Wan, M.; Jin, D.; Feng, R.; Si, L.; Gao, M.; Yue, L. *Inorg. Chem. Commun.* **2011**, *14*, 38.
(25) Morcrette, M.; Rozier, P.; Dupont, L.; Mugnier, E.; Sannier, L.; Galy, J.; Tarascon, J. M. *Nat. Mater.* **2003**, *2*, 755.
(26) Morales, J.; Sánchez, L.; Martín, F.; Ramos-Barrado, J. R.; Sánchez, M. *Electrochim. Acta* **2004**, *49*, 4589.
(27) Souza, E. A.; Landers, R.; Cardoso, L. P.; Cruz, T. G. S.; Tabacniks, M. H.; Gorenstein, A. *J. Power Sources* **2006**, *155*, 358.
(28) Maier, J. *Nat. Mater.* **2005**, *4*, 805.
(29) Gao, X. P.; Bao, J. L.; Pan, G. L.; Zhu, H. Y.; Huang, P. X.; Wu, F.; Song, D. Y. *J. Phys. Chem. B* **2004**, *108*, 5547.
(30) Chen, L. B.; Lu, N.; Xu, C. M.; Yu, H. C.; Wang, T. H. *Electrochim. Acta* **2009**, *54*, 4198.
(31) Wang, L. L.; Gong, H. X.; Wang, C. H.; Wang, D. K.; Tang, K. B.; Qian, Y. T. *Nanoscale* **2012**, *4*, 6850.
(32) Park, J. C.; Kim, J.; Kwon, H.; Song, H. *Adv. Mater.* **2009**, *21*, 803.
(33) Wu, R. B.; Qian, X. K.; Yu, F.; Liu, H.; Zhou, K.; Wei, J.; Huang, Y. Z. *J. Mater. Chem. A* **2013**, *1*, 11126.